ACS OMEGA

http://pubs.acs.org/journal/acsodf

Article

RF Sputtered Nb-Doped MoS_2 Thin Film for Effective Detection of NO_2 Gas Molecules: Theoretical and Experimental Studies

Sankar Ganesh Ramaraj,* Srijita Nundy, Pin Zhao, Durgadevi Elamaran, Asif Ali Tahir, Yasuhiro Hayakawa, Manoharan Muruganathan, Hiroshi Mizuta, and Sang-Woo Kim

Cite This: *ACS Omega* 2022, 7, 10492−10501

Read Online

ACCESS | Metrics & More | Article Recommendations | Supporting Information

ABSTRACT: Doping plays a significant role in affecting the physical and chemical properties of two-dimensional (2D) dichalcogenide materials. Controllable doping is one of the major factors in the modification of the electronic and mechanical properties of 2D materials. MoS_2 2D materials have gained significant attention in gas sensing owing to their high surface-to-volume ratio. However, low response and recovery time hinder their application in practical gas sensors. Herein, we report the enhanced gas response and recovery of Nb-doped MoS_2 gas sensor synthesized through physical vapor deposition (PVD) toward NO_2 at different temperatures. The electronic states of MoS_2 and Nb-doped MOS_2 monolayers grown by PVD were analyzed based on their work functions. Doping with Nb increases the work function of MoS_2 and its electronic properties. The Nb-doped MoS_2 showed an ultrafast response and recovery time of t_{rec} = 30/85 s toward 5 ppm of NO_2 at their optimal operating temperature (100 °C). The experimental results complement the electron difference density functional theory calculation, showing both physisorption and chemisorption of NO_2 gas molecules on niobium substitution doping in MoS_2.

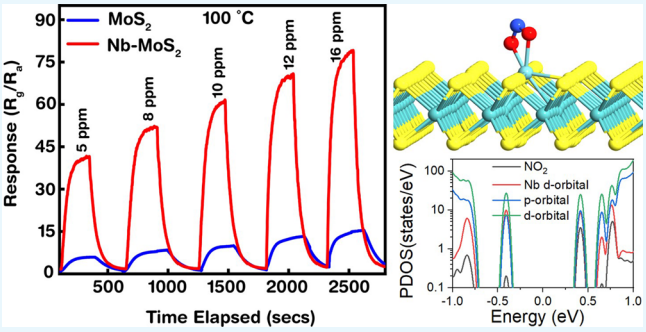

1. INTRODUCTION

Industrial technologies over the past several decades have significantly increased the amount of toxic gases in the atmosphere, which has dramatically affected the natural environment and human health.[1−3] Toxic gases in the atmosphere such as NO_2, SO_2, H_2S, CO, H_2, NH_3, and CH_4, can seriously affect human health and lead to global warming.[4−7] NO_2 has attracted significant attention because it can affect human health even at low ppb (parts per billion) levels. Moreover, inhalation of NO_2 leads to asthma, bronchitis, pulmonary edema, and respiratory problems.[8−11] Hence, real-time environmental monitoring of NO_2 gas sensors has become important in day-to-day life. Semiconductor gas detectors, electrochemical devices, mass sensors, and piezoelectric devices are normally utilized to monitor air quality. However, complex fabrication, low sensitivity, slow response, high power consumption, poor stability, and high device cost hinder these types of sensors in a wide range of applications.[5,7,12] This has stimulated researchers to focus on gas sensors with high response and selectivity. Recently, two-dimensional (2D) materials have gained considerable attention in gas sensing because of their physical and chemical properties.[13,14] Transition-metal dichalcogenide (TMD)-based materials are widely used in transistors, gas sensors, wearable devices, energy storage, and catalysis because of their unique thickness-dependent bandgap and excellent thermal properties.[13−17] TMDs particularly have large surface-area-to-bulk ratio thus enhance the adsorption of gases which can significantly modify their properties, making them promising materials for gas detection.[18,19] In particular, monolayer MoS_2 has attracted significant interest because of its direct bandgap of ≅1.83 eV and has proved to be versatile material for a wide range of applications in sensors.[18,19] Monolayer MoS_2 consists of three atomic layers, covalently bonded Mo and six S atoms, forming a sandwiched structure. However, the absence of a dangling bond in defect-free monolayer MoS_2 leads to chemically inert, terminal by S atoms.[20] Various methods, especially the introduction of defects and metal dopants have been explored, that improve the chemical activity and sensitivity of the basal plane of the MoS_2 monolayer.[20−22] Jia et al. investigated the theoretical structural stability and gas adsorption of monolayer MoS_2 doped with V, Nb, and Ta. They showed that this doping can significantly improve the adsorption of gas molecules.[20] Suh et al. synthesized Nb-doped MoS_2 by substitution cation doping, which is highly stable for the adsorption of volatile species.[23]

Received: January 2, 2022
Accepted: March 2, 2022
Published: March 15, 2022

https://doi.org/10.1021/acsomega.1c07274
ACS Omega 2022, 7, 10492−10501

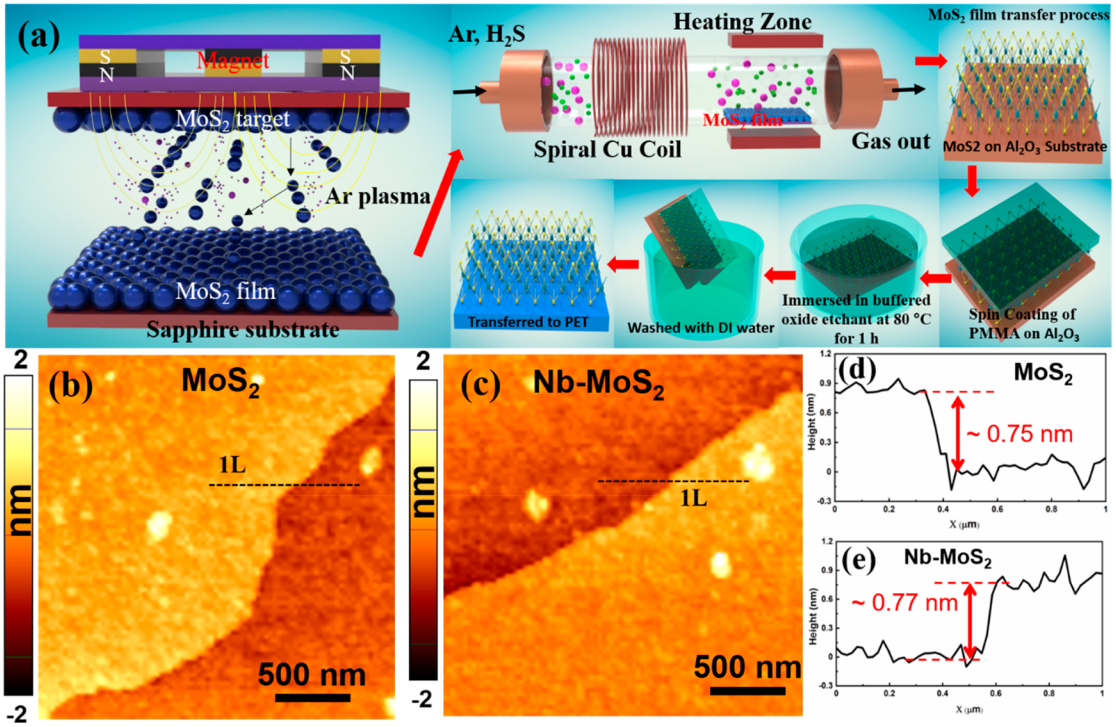

Figure 1. (a) Schematic representation of fabrication and transfer process of monolayer MoS_2 and Nb-doped MoS_2 using the RF magnetron sputtering technique. (b–e) AFM image and line profile analysis of MoS_2 and Nb doped MoS_2.

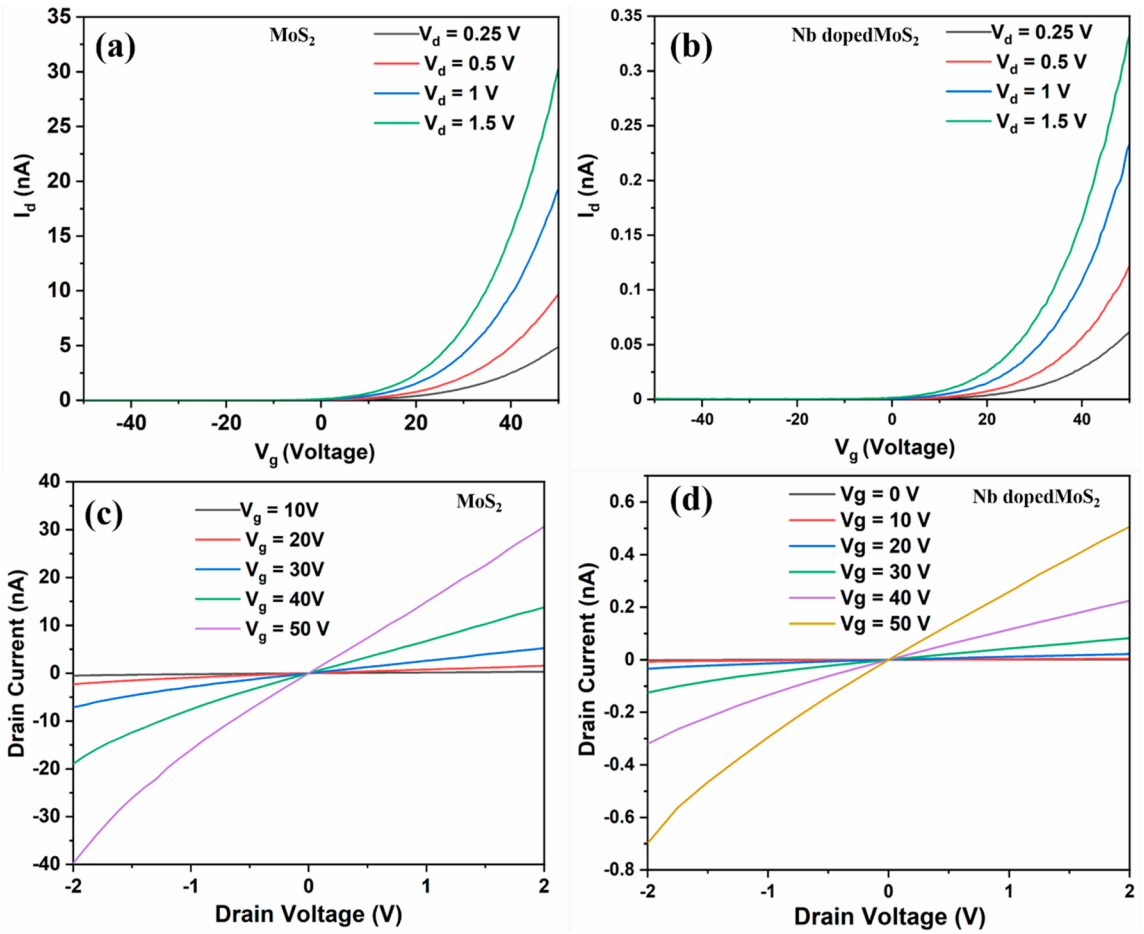

Figure 2. (a, b) I_d vs V_g characteristics of monolayer MoS_2 and Nb doped MoS_2 (linear scale). (c, d) I_d vs V_d characteristics of monolayer MoS_2 and Nb-doped MoS_2.

https://doi.org/10.1021/acsomega.1c07274
ACS Omega 2022, 7, 10492–10501

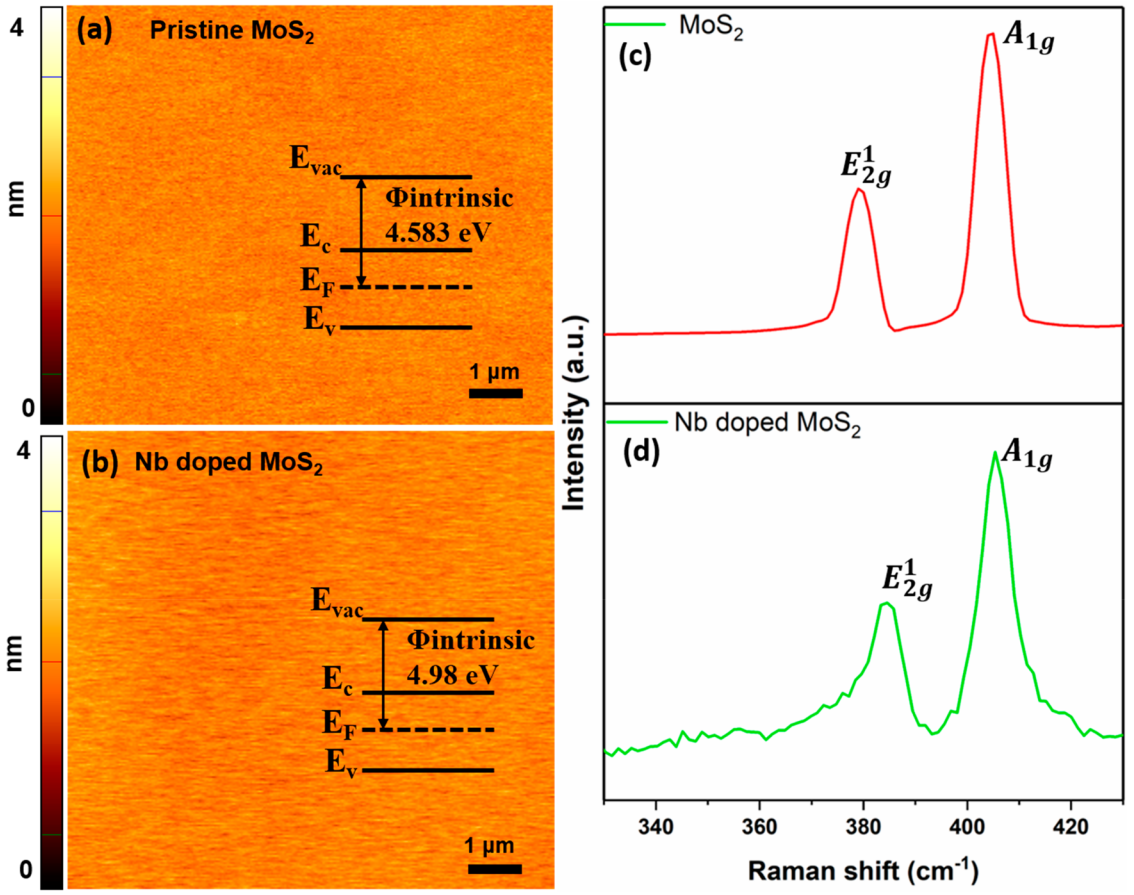

Figure 3. (a, b) KPFM image and band diagrams of pristine MoS_2 and Nb-doped MoS_2. (c, d) Raman spectrum of MoS_2 and Nb-doped MoS_2.

Doping with V and Cr in monolayer MoS_2 has been studied by Alex et al., showed that doping affected the electronic and mechanical properties of monolayer MoS_2.[24] This means that doping with metals improves the physical and chemical properties of monolayer MoS_2.[25] Nb is a transition metal with good solubility and one less d-orbital electron occupancy than Mo. Doping MoS_2 with Nb results in the injection of a high concentration of hole carriers. In addition, MoS_2 and NbS_2 have similar lattice parameters which do not cause a significant change in the lattice structure even when a NbS_2 covalent bond is formed.[26−29] The incorporation of metals such as Nb or V should enhance the strong interaction between the metal and gas molecules (NO_2). Thus, such dopant materials promise to enhance the selectivity and gas response of monolayer MoS_2 gas sensors.[20] However, Nb-doped MoS_2 monolayer NO_2 gas sensors have not yet been reported. Herein, we present theoretical and experimental investigations on the adsorption properties of monolayer MoS_2 and Nb-doped MoS_2 for gas molecules (acetone, NH_3, toluene, NO_2, and CO). Controlled doping of the Nb-doped MoS_2 monolayer was performed using a physical vapor deposition (PVD) method. Furthermore, we demonstrated the behavior of doped and undoped MoS_2 gas sensors toward different concentrations of NO_2 at 100 °C. Finally, we report on density functional theory (DFT) simulations to understand the adsorption energetics and changes in the electronic structure of MoS_2 and Nb-doped MoS_2 after interaction with NO_2 gas molecules. DFT simulation complements the experimental results and also helps to understand the gas-sensing mechanism of MoS_2 and Nb-doped MoS_2.

2. RESULTS AND DISCUSSION

A MoS_2 and Nb-doped MoS_2 monolayer was fabricated using radio frequency (RF)-sputtering and was transferred onto the bare polyethylene terephthalate (PET) substrate, as shown in the schematic representation in Figure 1 and verified by atomic force microscope (AFM). The thickness of MoS_2 and Nb-doped MoS_2 was approximately 0.75 and 0.77 nm, as shown in Figure 1b−e. Figure S1a,b shows the SEM top view and energy dispersive X-ray analysis (EDX) of MoS_2 and Nb-doped MoS_2 fabricated device. The result shows that the perfect nanochannel is made up from the monolayer MoS_2 and Nb-doped MoS_2 thin film. EDX analysis reveals the presence of Nb, Mo, and S elements in the RF sputtered monolayer thin film. We have analyzed the electrical transport of MoS_2 and Nb-doped MoS_2 fabricated devices, as shown in Figure 2. The results indicate that the current of Nb-doped MoS_2 has sharply decreased compared with pure MoS_2, which indicates that substitutional Nb doping significantly increased hole injection and also suppressed the heavily n-type MoS_2 characteristics (Figure 2a,b). Moreover, the slight movement in the threshold voltage to positive voltage indicated the doping of Nb in the MoS_2 monolayer. Figure 2c,d shows $I-V$ curves of MoS_2 and Nb-doped MoS_2 by applying different gate biases (0 to 50 V), the results indicate that restraint of electrical transport conductivity with Nb doping.[25] The electronic states of the MoS_2 and Nb-doped MoS_2 thin films were investigated using Kelvin probe force microscopy (KPFM). The work function of MoS_2 increased from 4.583 ± 0.005 to 4.98 ± 0.005 eV, and the new states were formed near the valence band, maximum owing to substitution doping of Nb

https://doi.org/10.1021/acsomega.1c07274
ACS Omega 2022, 7, 10492−10501

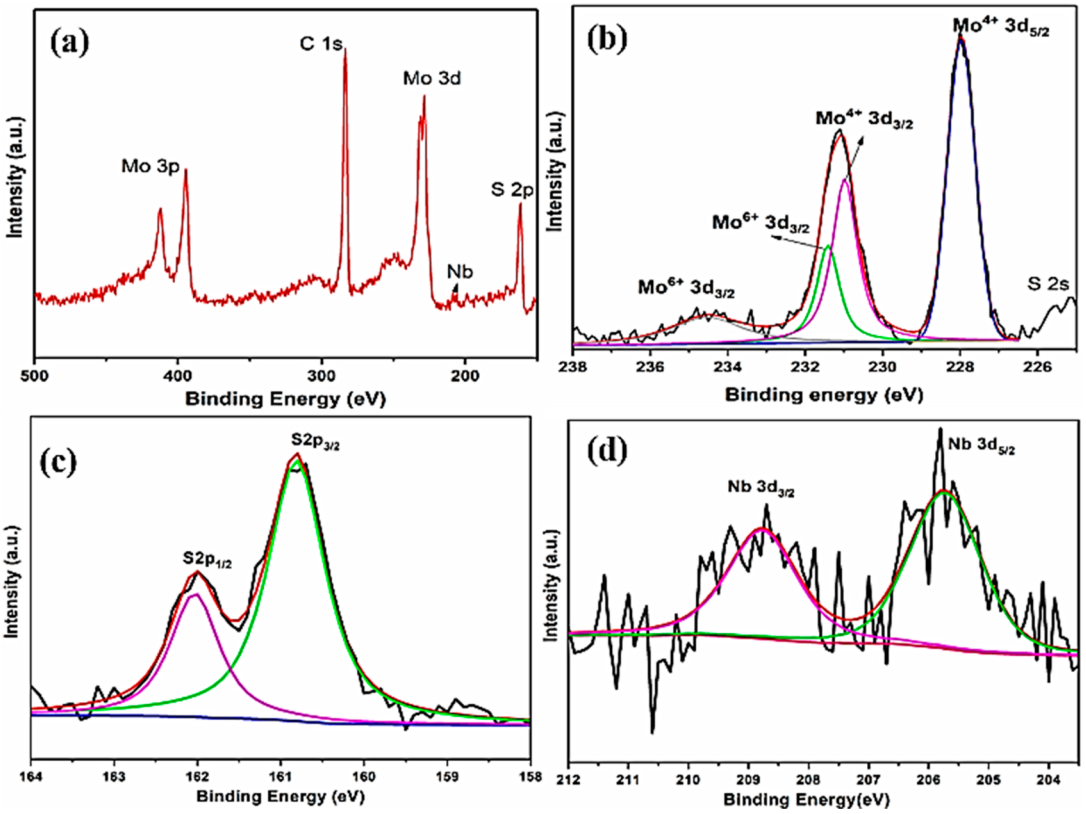

Figure 4. (a) Wide spectrum of Nb-doped MoS_2. (b, c) XPS spectra of Mo 3d and S 2p of Nb-doped MoS_2. (d) XPS spectrum of Nb 3d.

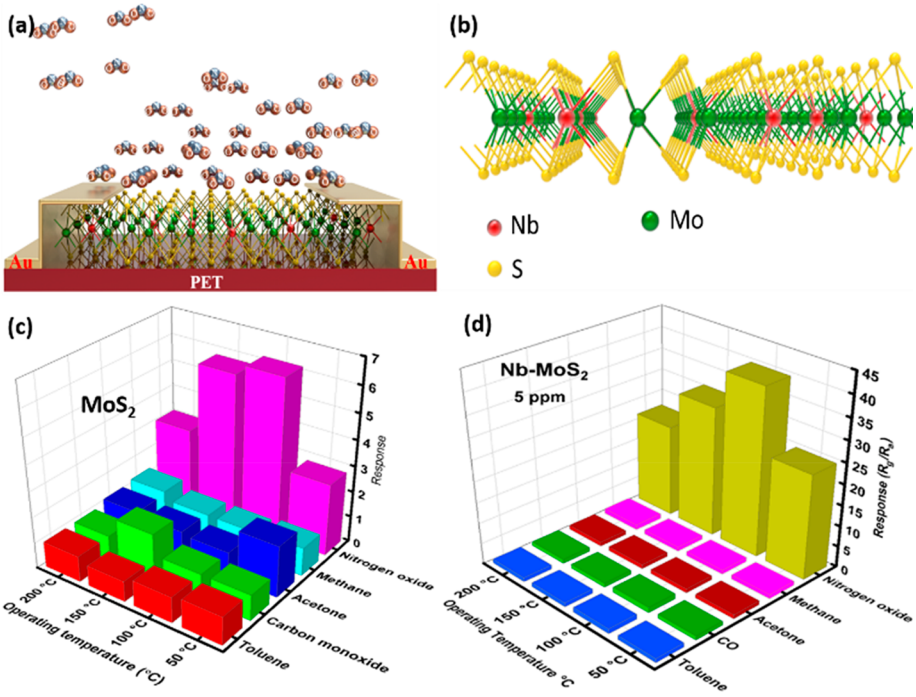

Figure 5. (a) Schematic representation of Nb-doped MoS_2 device under NO_2 gas sensor. (b) Crystal structure in which Nb is doped in the substitutional sites of Mo. (c, d) Selectivity of MoS_2 and Nb-doped MoS_2.

in the MoS_2 films (Figure 3a,b). Raman spectroscopy analysis was performed to determine the formation of monolayer MoS_2 and Nb-doped MoS_2. As shown in Figure 3c,d, two major peaks at 384 and 404 cm^{-1} were observed in the samples, corresponding to in-plane E^1_{2g} and out-of-plane A^1_g vibrations of Nb-doped MoS_2. The distance between the vibrational peaks was 20 cm^{-1}, which indicates the formation of monolayer MoS_2 that agrees with the AFM image.[30,31]

X-ray photoelectron spectroscopy (XPS) analysis was performed to determine the oxidation state of the elements via

https://doi.org/10.1021/acsomega.1c07274
ACS Omega 2022, 7, 10492−10501

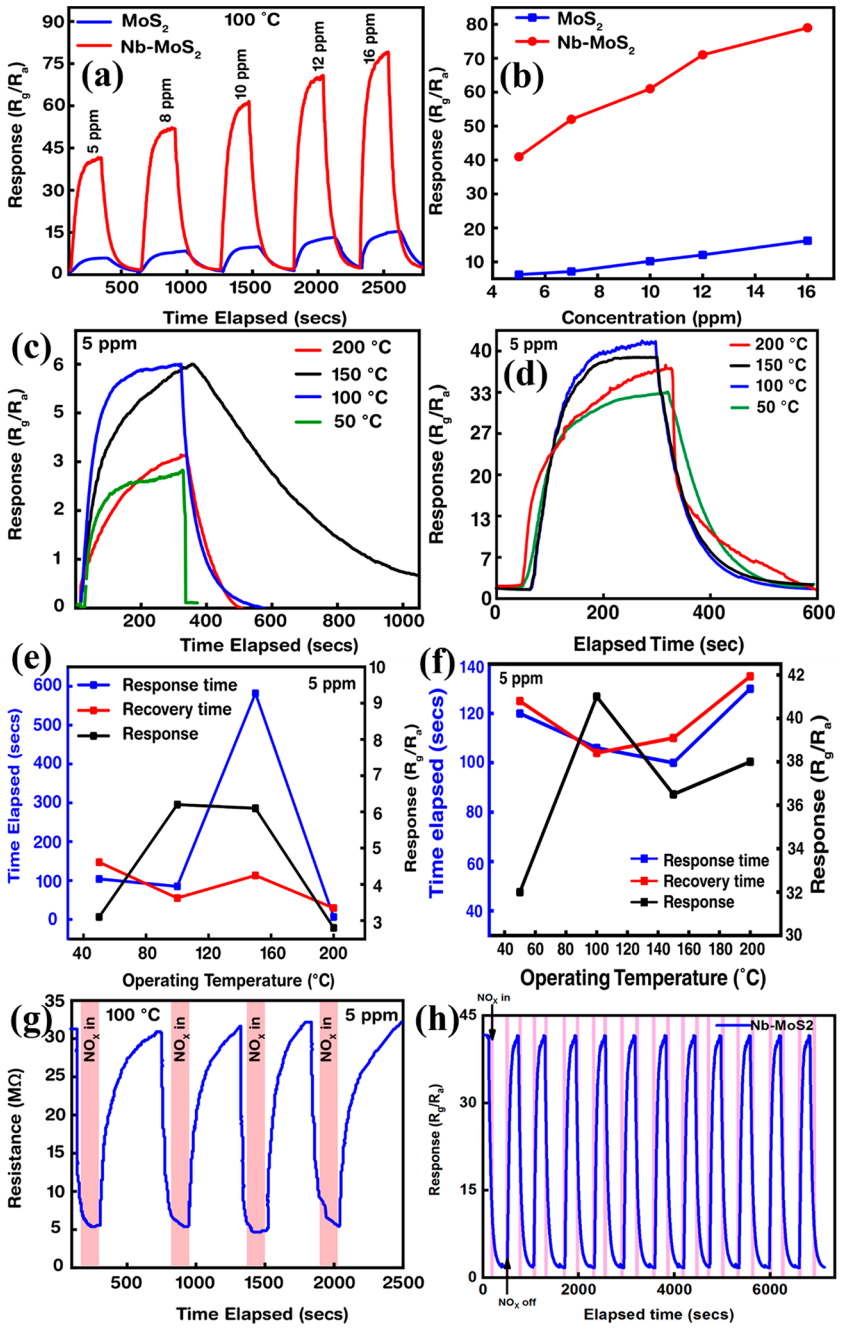

Figure 6. Measurement of sensing performance: (a, b) Dynamic response and recovery curves of MoS_2 and Nb-doped MoS_2 to various concentrations of NO_2. (c, d) Gas response curve of MoS_2 and Nb-doped MoS_2 at different temperature. (e, f) Response and recovery times toward 5 ppm at different operating temperatures for both samples. (g, h) Several cycles to determine the repeatability in detection of NO_2 for MoS_2 and Nb-doped MoS_2.

binding energy and surface element composition. Binding energies have distinct values for each element, which are used to identify the individual elements in materials. Figure 4 shows the high-resolution spectra of Mo 3d, Nb 3d, and S 2s core levels. Figure 4a illustrates the wide spectra of Nb-doped MoS_2 which clearly indicates the presence of Nb, Mo, S, and C. Three major peaks are featured at 228.1 eV (Mo $3d_{5/2}$), 231.2 eV (Mo $3d_{3/2}$), and 225.5 eV (S 2s) as shown in Figure 4b. The intense peak at 228.1 eV is attributed to Mo^{4+} (i-Mo^{4+}) and the charge state of molybdenum in Nb-doped MoS_2. The binding energy at 234.5 eV is due to Mo^{6+} of the unreacted precursor of MoO_3, which may be a contaminant in the Nb-doped MoS_2.[32−35] The peak at 225.5 eV is due to an overlapping S 2s peak, corresponding to sulfur close to a defect, which agrees well with the previous reports.[26] The sulfur environment can be more clearly studied by employing the S 2p core level spectrum, as shown in Figure 4c, and the convoluted XPS shows two doublet peaks at 160.8 and 161.9 eV, respectively. The higher binding energy (160.8 eV) is attributed to sulfur vacancies (d-s) and the lower binding energy to intrinsic S.[35−38] The convoluted XPS spectrum of Nb 3d is composed of doublets attributed to the spin−orbital splitting of $3d_{5/2}$ (205.7 eV) and $3d_{3/2}$ (208.7 eV), as depicted in Figure 4d. The results indicate that the as-grown Nb-doped MoS_2 has a uniform high-quality intrinsic structure on the substrate.[23]

https://doi.org/10.1021/acsomega.1c07274
ACS Omega 2022, 7, 10492−10501

We fabricated a flexible monolayer gas sensor on PET substrate, as shown in the schematic representation in Figure 5a,b, and investigated the gas sensing behavior of MoS_2 and Nb-doped MoS_2 toward NO_2 gas in air atmosphere at different temperatures. First, the relative responses of MoS_2 and Nb-doped MoS_2 gas sensors to different gas at various temperatures were examined. From Figure 5c,d, it was observed that the MoS_2 and Nb-doped MoS_2 showed higher response toward NO_2 than other gases. In addition, the selectivity of both sensing materials were evaluated to determine the efficiency of the sensor. The selectivity of the as-synthesized sensing materials was examined at different operating temperatures (50−200 °C) for the most commonly interfering gases such as toluene, CO, acetone, and NH_3 in an air atmosphere. The resistance change was assessed at 5 ppm concentration for each target gas, and the results indicated the highly selective nature of monolayer MoS_2 and Nb-doped MoS_2 toward NO_2 gas compared with other gases. It was observed that monolayer MoS_2 showed a slight response to the interfering gases, and the observed response values were 2.2 (150 °C) and 2.35 (50 °C) for CO and acetone, respectively. However, Nb-doped MoS_2 showed high selectivity to NO_2 and no response (S = 1) to the interfering gases, making the Nb-doped MoS_2 sensor selectively operable during low-temperature operation for NO_2 detection even when it coexists with other reducing gases in the air. Figure 6a compares the typical dynamic gas response−recovery characteristics of monolayer MoS_2 and Nb-doped MoS_2 gas sensors with different concentrations of NO_2 gas exposure at 100 °C. The gas response is represented in by normalized change in resistance of the sensor. For monolayer MoS_2, the corresponding gas response values to 5, 7, 10, 12, and 16 ppm of NO_2 gas were noted to be 5.2, 8.1, 10.5, 12.35, and 16.23, respectively. Notably, the gas response of the Nb-doped MoS_2 monolayer was enhanced compared to that of the undoped monolayer MoS_2 over the full gas concentration range. The corresponding gas response values for the same sequence of NO_2 gas concentrations were 40.22, 50.12, 61, 70.9, and 80.5, respectively. Figure 6b shows the estimated sensitivity (S) of Nb-doped MoS_2 (S = 10) to be higher than that of undoped MoS_2 monolayer (S = 2), and a linear trend is observed for the undoped MoS_2 sensor as compared to Nb-doped MoS_2, where a slightly curved fitting is observed. In addition, undoped MoS_2 showed a good response to 3 ppm of NO_2 in air (Figure S2). Figure 6c shows the dynamic gas-sensing response and recovery curves of monolayer MoS_2 upon exposure to 5 ppm of NO_2 at operating temperatures of 50, 100, 150, and 200 °C. Monolayer MoS_2 showed an increased sensing response at 100 °C compared to other temperatures, along with rapid recovery upon the exclusion of NO_2. However, when the temperature rose beyond 150 °C, there was a gradual decrease in the gas response due to the significant desorption rate compared to the adsorption rate (representing a typical volcano curve). In addition, the low desorption rate of the molecules at a lower temperature of MoS_2 may be due to the high binding energy of NO_2 or strong bonding between NO_2 and MoS_2. At lower temperatures, the chemical activity of NO_2 gas molecules on the MoS_2 surface is relatively low, which leads to a low response. At the optimum temperature (100 °C), the desorption rate of the NO_2 gas molecules enhances the recovery from the Nb-MoS_2 by removing accumulated moisture before reacting with targeted gas and initiating the surface catalyst at elevated temperatures. However, a further increase in temperature leads to a quick reaction and penetration of NO_2 gas molecules in the Nb-MoS_2-sensing film, which results in a decrease in the gas response.[39,40]

Further, Figure 6d shows the dynamic gas sensing response and recovery curves of Nb-doped MoS_2 upon exposure to 5 ppm of NO_2 at different operating temperatures of 50, 100, 150, and 200 °C. Compared to monolayer MoS_2, Nb-doped MoS_2 shows a significant increase in sensing response to 5 ppm of NO_2 with an enhanced stable behavior at 100 °C compared to that at other temperatures. A trend similar to that observed in monolayer MoS_2 with a decrease in gas response beyond 100 °C was seen in the sensing performance of Nb-doped MoS_2. However, Nb-doped MoS_2 displayed a higher and stable response with almost full recovery when compared to monolayer MoS_2, suggesting that doping with Nb plays a significant role in gas sensing enhancement. We further investigated the time required for both samples to acquire 90% response and recovery on gas exposure and removal, respectively, at different operating temperatures. The transient dynamic response of the monolayer MoS_2 and Nb-doped MoS_2 sensors in Figure 6e,f shows that the corresponding response−recovery times are (t_{res} = 110/80 s) and (t_{rec} = 30/85 s) toward 5 ppm of NO_2 at their optimal operating temperature (100 °C). The Nb-doped MoS_2 sensor displays a faster response and more stable recovery than monolayer MoS_2. To further verify the stability and reproducibility of the sensors, both sensors were kept in ambient conditions and inspected after one month. Both monolayer MoS_2 and Nb-doped MoS_2 sensors were subjected to 4 and 10 reversible cycles (each cycle comprised of one response and recovery process) under exposure to 5 ppm of NO_2 at 100 °C, as displayed in Figure 6g,h. The response was similar for each cycle. Furthermore, both sensors displayed excellent stability and reversibility in each cycle. In Figure 6g, the sensor response of monolayer MoS_2 toward 5 ppm of NO_2 at 100 °C for each cycle was 5.2, 4.96, 5.42, and 4.98, which can be considered a very stable response. Figure 6h shows that Nb-doped MoS_2 exhibited a highly stable sensing behavior toward 5 ppm of NO_2 at 100 °C with cycle responses of 40.22, 40.48, 40.52, and 39.95, which is <2% variability. These results reveal that the sensor has good stability toward NO_2 gas. The results of previously reported MoS_2 gas sensors are compared with those of our gas sensor are shown in Table 1.[41−47]

Table 1. Comparison between the Literature-Based MoS_2 Gas Sensors and Present Work

sensing materials	S (%)	NO_2 conc. ppm	T (°C)	t_{res} (s)	t_{rec} (s)	ref
MoS_2 aerogel	12	0.5	200	33	107	41
MoS_2/Pt	18	5	–	1600	1600	42
atomic layered MoS_2	25	50	100	–	–	43
MoS_2 monolayer	12	5	100	71	310	1
MoS_2 hallow sphere	40.3	100	150	79	225	44
graphene/MoS_2	8	5	150	–	–	45
sputtered MoS_2	32	100	150	56	80	46
MoS_2 nanowire	2	1	120	16	172	47
Nb-MoS_2	44	5	100	30	85	this work

To date, the exact gas-sensing mechanism is unknown, but in this work, its elucidation is based on the degree of charge perturbation on the surface between NO_2 and monolayer MoS_2 interaction. The change in the resistance of MoS_2 directly corresponds to the concentration and the amount of adsorption of NO_2 gas molecules on the MoS_2 surface. The gas-sensing

https://doi.org/10.1021/acsomega.1c07274
ACS Omega 2022, 7, 10492−10501

properties are strongly affected by the surface stoichiometry and the intrinsic properties of MoS_2. The mechanism of gas sensing is briefly explained below with the help of DFT.

DFT Study of Adsorption of NO_2 Molecules. Initially, the atomic structure of Nb atoms placed in the sulfur vacancy position of MoS_2 (MoS_2-S-Vac-Nb) and substitutional Nb atoms in the Mo atom location of MoS_2 (MoS_2-Mo-Subs-Nb) were optimized by fully relaxing the atomic structure until the remaining residual force is smaller than 0.05 eV/Å. In the resultant atomic structure of Nb-doped MoS_2, a NO_2 molecule was adsorbed and then optimized as shown in Figure 7c,e.

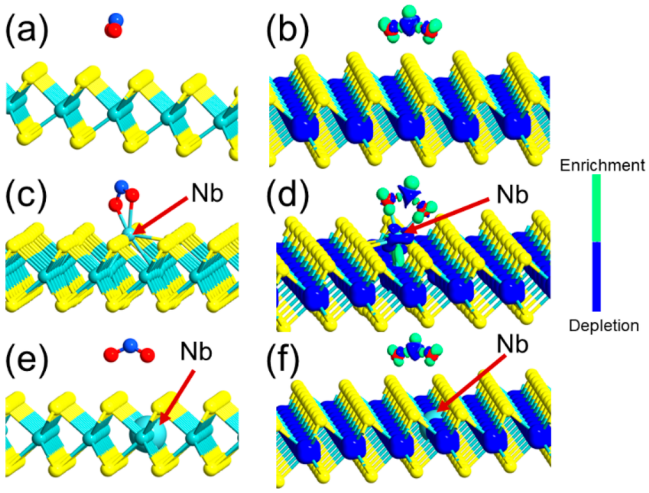

Figure 7. Geometrically optimized atomic configuration of (a) MoS_2-NO_2, (c) Nb-doped in sulfur vacancy MoS_2-NO_2, and (e) substitutional Nb-doped in Mo atom position of MoS_2-NO_2. These electron difference density isosurface plots are shown in (b), (d), and (f), respectively. Isovalue: 0.11 e/Å^3.

Similarly, the MoS_2-NO_2 structure was geometrically optimized to have a residual force smaller than 0.05 eV/Å. Figure 7a shows the geometrically optimized MoS_2-NO_2 atomic structure. The binding energy of the NO_2 molecule on the MoS_2 or Nb-doped MoS_2 supercell is calculated as $E_{bind} = E_{(MoS_2/Nb\text{-}NO_2)} - (E_{MoS_2/Nb} + E_{NO_2})$, where $E_{(MoS_2/Nb\text{-}NO_2)}$ is the total energy of the NO_2 molecule adsorbed on MoS_2 or MoS_2Nb-doped supercells, $E_{MoS_2/Nb}$ is the total energy of the MoS_2 or MoS_2Nb-doped supercells, and E_{NO_2} is the total energy of the NO_2 molecule. The calculated binding energies for MoS_2-NO_2, MoS_2-S-Vac-Nb-NO_2, and MoS_2-Mo-Subs-Nb-NO_2 atomic structures are −0.681, −3.9, and −0.658 eV, respectively. These binding energies indicate that (i) the NO_2 molecule is physisorbed onto MoS_2 and MoS_2-Mo-Subs-Nb atomic structures and (ii) NO_2 molecules are chemically bonded onto the Nb-doped sulfur vacancy of MoS_2 as the binding energy is higher than 1.0 eV. In the experimental work, the sensors were recovered after NO_2 sensing measurements, which indicates that NO_2 molecules were physisorbed onto Nb-doped MoS_2. This analysis rules out the possibility of using Nb-doped sulfur vacancy MoS_2 crystals in sensing measurements. To assess the amount of charge and transfer between NO_2 molecules and MoS_2 or Nb-doped MoS_2 channels, Mulliken population analysis was performed. It was found that the NO_2 molecules accept 0.066, 0.198, and 0.009 electrons for MoS_2-NO_2, MoS_2-S-Vac-Nb-NO_2, and MoS_2-Mo-Subs-Nb-NO_2 atomic structures, respectively. The electron difference density plots are shown in Figure 7b,d,f, depicting this charge transfer process. In the case of MoS_2-NO_2 and MoS_2-Mo-Subs-Nb-NO_2 structures, charge transfer from the MoS_2 layer to NO_2 molecules occurs via the van der Waals bonding. For the MoS_2-S-Vac-Nb-NO_2 system, chemical bonding-induced charge transfer happens.

To understand the atomistic origin of the high sensing response of Nb-doped MoS_2 channel, the total density of states (TDOS) and projected density of states (PDOS) analyses were carried out. Figures 8a,b show that NO_2 adsorption leads to p-

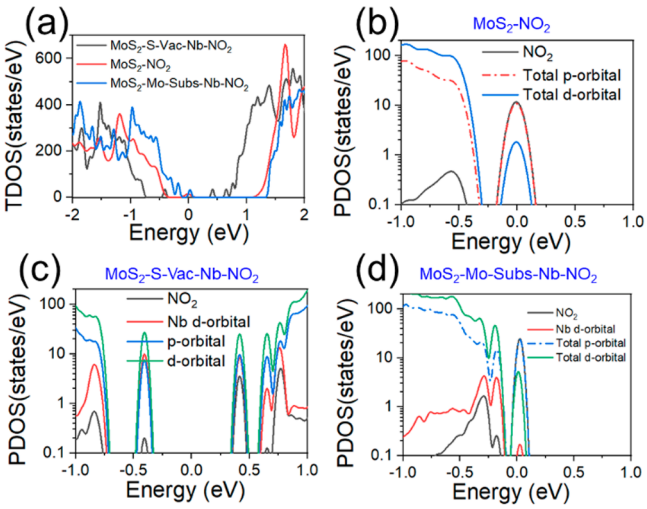

Figure 8. (a) TDOS plot of MoS_2-NO_2, Nb-doped in sulfur vacancy MoS_2-NO_2, and substitutional Nb-doped in Mo atom position of MoS_2-NO_2 and their PDOS in (b), (c), and (d), respectively.

type doping in MoS_2 and substitutional Nb in the Mo position of MoS_2 (MoS_2-Mo-Subs-Nb) channels. Furthermore, Nb doping in the sulfur vacancy position of MoS_2 (MoS_2-S-Vac-Nb) does not show p-doping characteristics, which is attributed to the formation of stable chemical bonds. In the case of the MoS_2-NO_2 structure, the NO_2 molecule orbitals hybridize with the d-orbitals of MoS_2 close to the Fermi energy (Figure 8c). In the MoS_2-Mo-Subs-Nb-NO_2 system, Nb d-orbitals hybridize well with the p- and d-orbitals of MoS_2. Additionally, these d-orbitals strongly hybridize with NO_2 molecule orbitals around the Fermi energy, as shown in Figure 8d. Owing to this well-localized hybridization, more scattering occurs in the experimental results.

In addition, oxygen atoms of the NO_2 molecule move closer to the sulfur atoms of MoS_2 (shown in Figure S3). The charge transfer of 0.009 electrons transfer indicates that scattering is dominant rather than doping. These characteristics lead to high response to NO_2 sensing in the Nb-doped MoS_2 channel.[48−54]

From the above experimental and theoretical studies, we propose the gas sensing mechanism as follows. The adsorption of NO_2 gas molecules on Nb-doped MoS_2 prefers to be physisorbed on the Nb-MoS_2surface via the two oxygen atoms. These oxygen atoms bound to the metal sites by forming an M−O−N−O four numbered ring structure. The DFT analysis showed higher adsorption energy for Nb-doped MoS_2, which suggests that the doping Nb center can drastically enhance the adsorption of gas molecules due to the catalytic activity. In addition to this, the Nb metal center has strong activation energy to attract the NO_2 gas molecules. This leads to the enhanced gas response, reproducibility, and stability of the Nb-doped gas sensor. However, in the case of an undoped MoS_2 monolayer, the interaction between the NO_2 gas molecules and MoS_2 is

https://doi.org/10.1021/acsomega.1c07274
ACS Omega 2022, 7, 10492−10501

weak with low corresponding adsorption energy, which leads to poor gas response and stability. In addition, in an oxygen environment, a p-type doping effect is observed owing to the extraction of electrons from MoS_2. Hence, the absorbed oxygen extracts electrons from the MoS_2 and formed O_2^- ions, as shown in the following equations:[1,55,56]

$$O_2(gas) \rightarrow O_2(ads) \quad (1)$$

$$O_2(ads) + e^- \rightarrow O_2^-(ads) \quad (2)$$

$$NO_2(gas) + e^- \rightarrow NO_2^-(ads) \quad (3)$$

The electron carrier density of MoS_2 decreased due to the depletion of its electrons by atmospheric oxygen. Moreover, the several reactive sites in MoS_2 are occupied by oxygen molecules. Upon exposure to NO_2 at 100 °C, fewer gas molecules are absorbed on the surface, and there is less electron transfer due to the limited number of active sites. In addition, the interaction between oxygen molecules and the MoS_2 layer will be weak due to lower adsorption energy. This lower adsorption energy leads to less adsorption of oxygen molecules.

3. CONCLUSION

We showed the effect of the flexible Nb-doped gas-sensing properties of monolayer MoS_2 using the PVD method. The NO_2 gas sensing response was enhanced dramatically, by five times compared to an undoped MoS_2 monolayer, by employing the substitutional doping of Nb. In addition, Nb-doped MoS_2 showed excellent stability and reproducibility compared to undoped MoS_2. These effects on gas response and stability can be attributed to substitutional cation doping of Nb in the host MoS_2, which enhances the number of grains and surface-to-volume-ratio. In addition, the substitutional cation showed physisorption of NO_2, which induces faster response and recovery compared to the undoped monolayer MoS_2. We hope these results will be useful in understanding the role of Nb dopants (metals) in gas-sensing applications.

4. EXPERIMENTAL SECTION

Synthesis of Monolayer MoS_2 and Nb-Doped MoS_2. Nb-doped MoS_2 and MoS_2 were grown controllably on 1 cm × 1 cm sapphire (Al_2O_3) substrates, using a 4-in. pure MoS_2 target (MoS2, 99.9%) and Nb-doped MoS_2 targets (5%: 95%) by PVD at 700 °C for 30 s. Prior to the growth of monolayer MoS_2, the sapphire substrate was cleaned by using a standard chemical process. The substrate was placed precisely in a face-down position in the chamber. Approximately 30 W of RF power was utilized to sputter monolayer MoS_2 under an Ar (13 sccm) flow atmosphere, and the working pressure was approximately 1 Pa during the sputtering process. The samples were postannealed at 1000 °C in an H_2S (5 sccm)/Ar (80 sccm) atmosphere for 30 min.

Transfer of MoS_2 and Nb-Doped MoS_2 Thin Film onto a PET Substrate. The MoS_2 thin film formed on the sapphire substrate was spin-coated with a poly(methyl methacrylate) (PMMA) solution. The substrate was then dried at 120 °C on the hot plate for 2 min. A few hours later, the substrate was immersed in a buffered oxide etchant (NH_4F:HF, 6:1) solution at 80 °C for 1 h. After etching the substrate, MoS_2/PMMA was transferred to deionized water several times to remove the buffer solution. Finally, the delaminated MoS_2/PMMA was transferred onto a PET substrate. PMMA was removed by immersing the PET substrate in acetone for 5 min.

Characterization and Sensor Fabrication. The thicknesses of the MoS_2 and Nb-doped MoS_2 monolayer were measured using an AFM system (XE100, Park Systems) in contact mode under a contact force of 30 nN and at a scan rate of 0.5 Hz. Raman analysis was performed using a JASCO NR1800 Raman spectrometer equipped with a Nd:YAG laser. The deposited Au/Ti/Cr electrodes with a length and thickness of 50 μm were deposited by using photolithography and electron beam evaporation. The thicknesses of the coated Au (40 nm), Ti (8 nm), and Cr (2 nm).

Gas Sensing Measurement. Gas sensing tests were conducted using our in-house gas sensing system. Gas sensing characteristics were investigated using nitrogen oxide (NO_2), toluene ($C_6H_5CH_3$), carbon monoxide (CO), and acetone (CH_3COCH_3), diluted with synthetic air using mass flow controllers. Joule heating was used to control the operating temperature of the gas sensors by using a ceramic heater connected to a power supply and varying the temperature from 50 to 200 °C. The responses of each test were defined as R_g/R_a or R_a/R_g when they were reacted with oxidizing or reducing gases, respectively, where R_a and R_g represent resistance in ambient and analyte gas, respectively. In addition, the response and recovery times for each test were determined by calculating the time for both the ambient and analyte gas atmospheres. The schematic representation of the gas sensing setup is shown in the Figure S4

DFT Simulation. DFT calculations were performed using the Quantum ATK DFT package,[53,54] which is based on a linear combination of numerical atomic orbitals. FHI pseudopotentials with double-ζ double polarized basis sets are employed. To account for the long-range van der Waals interactions more accurately, Grimme DFT-D3 van der Waals corrections were utilized.[54] The revised Perdew−Burke−Ernzerhof exchange−correlation functional was used to obtain a more accurate molecule to MoS_2 layer distance and binding energy. A 20 Å vacuum distance was used above and below the MoS_2 layer to overcome any spurious interactions with the adjacent supercell. MoS_2 supercell dimensions of 31.604 Å × 27.3698 Å × 30 Å were employed in these simulations. A density mesh cutoff of 75 Ha was used.

■ ASSOCIATED CONTENT

Supporting Information

The Supporting Information is available free of charge at https://pubs.acs.org/doi/10.1021/acsomega.1c07274.

SEM image of and EDX anlaysis of MoS_2 and Nb-doped MoS_2 (Figure S1); dynamic response curve of Nb-doped MoS_2 (Figure S2); theoretical calculation of MoS_2 and Nb doped MoS_2 toward NO_2; schematic representation of Gas sensing setup (PDF)

■ AUTHOR INFORMATION

Corresponding Author

Sankar Ganesh Ramaraj − *School of Materials Science, Japan Advanced Institute of Science and Technology, Nomi 923-1211, Japan;* orcid.org/0000-0002-6837-9112; Email: sankarg27@gmail.com, ramaraj@jaist.ac.jp

Authors

Srijita Nundy − *College of Engineering, Mathematics and Physical Sciences, Renewable Energy, University of Exeter, Penryn, Cornwall TR10 9FE, United Kingdom*

https://doi.org/10.1021/acsomega.1c07274
ACS Omega 2022, 7, 10492−10501

Pin Zhao − *School of Advanced Materials Science and Engineering, Sungkyunkwan University, Suwon 16419, Republic of Korea*
Durgadevi Elamaran − *Graduate School of Science and Technology, Shizuoka University, Hamamatsu 432-8011, Japan*
Asif Ali Tahir − *College of Engineering, Mathematics and Physical Sciences, Renewable Energy, University of Exeter, Penryn, Cornwall TR10 9FE, United Kingdom;* orcid.org/0000-0003-1985-6127
Yasuhiro Hayakawa − *Research Institute of Electronics, Shizuoka University, Hamamatsu 432-8011, Japan*
Manoharan Muruganathan − *School of Materials Science, Japan Advanced Institute of Science and Technology, Nomi 923-1211, Japan;* orcid.org/0000-0001-5421-5160
Hiroshi Mizuta − *School of Materials Science, Japan Advanced Institute of Science and Technology, Nomi 923-1211, Japan*
Sang-Woo Kim − *School of Advanced Materials Science and Engineering, Sungkyunkwan University, Suwon 16419, Republic of Korea;* orcid.org/0000-0002-0079-5806

Complete contact information is available at: https://pubs.acs.org/10.1021/acsomega.1c07274

Notes

The authors declare no competing financial interest.

■ ACKNOWLEDGMENTS

The authors acknowledge the support by (1) a Grant-in-Aid for Scientific Research (Early Career Scientists) (21K14510) from the Japan Society for the Promotion of Science (JSPS KAKENHI), (2) Japan Advanced Institute of Science and Technology, Japan and (3) Engineering and physical Science Research Council (EPSRC) under research grant no.EP/V049046/1

■ REFERENCES

(1) Kumar, R.; Goel, N.; Kumar, M. UV-Activated MoS2 Based Fast and Reversible NO2 Sensor at Room Temperature. *ACS Sensors* **2017**, *2* (11), 1744−1752.
(2) Aslam, M.; Chaudhary, V. A.; Mulla, I. S.; Sainkar, S. R.; Mandale, A. B.; Belhekar, A. A.; Vijayamohanan, K. A Highly Selective Ammonia Gas Sensor Using Surface-Ruthenated Zinc Oxide. *Sensors and Actuators A: Physical* **1999**, *75* (2), 162−167.
(3) Singh, S.; Deb, J.; Sarkar, U.; Sharma, S. MoSe2 Crystalline Nanosheets for Room-Temperature Ammonia Sensing. *ACS Applied Nano Materials* **2020**, *3* (9), 9375−9384.
(4) Yi, N.; Cheng, Z.; Li, H.; Yang, L.; Zhu, J.; Zheng, X.; Chen, Y.; Liu, Z.; Zhu, H.; Cheng, H. Stretchable, Ultrasensitive, and Low-Temperature NO2 Sensors Based on MoS2@rGO Nanocomposites. *Materials Today Physics* **2020**, *15*, 100265.
(5) Xu, T.; Pei, Y.; Liu, Y.; Wu, D.; Shi, Z.; Xu, J.; Tian, Y.; Li, X. High-Response NO2 Resistive Gas Sensor Based on Bilayer MoS2 Grown by a New Two-Step Chemical Vapor Deposition Method. *J. Alloys Compd.* **2017**, *725*, 253−259.
(6) Yan, X.; Wu, Y.; Li, R.; Shi, C.; Moro, R.; Ma, Y.; Ma, L. High-Performance UV-Assisted NO2 Sensor Based on Chemical Vapor Deposition Graphene at Room Temperature. *ACS Omega* **2019**, *4* (10), 14179−14187.
(7) Sankar ganesh, R.; Navaneethan, M.; Mani, G. K.; Ponnusamy, S.; Tsuchiya, K.; Muthamizhchelvan, C.; Kawasaki, S.; Hayakawa, Y. Influence of Al Doping on the Structural, Morphological, Optical, and Gas Sensing Properties of ZnO Nanorods. *J. Alloys Compd.* **2017**, *698*, 555−564.
(8) Novikov, S.; Lebedeva, N.; Satrapinski, A.; Walden, J.; Davydov, V.; Lebedev, A. Graphene Based Sensor for Environmental Monitoring of NO2. *Sens. Actuators, B* **2016**, *236*, 1054−1060.
(9) Su, P. G.; Yu, J. H. Enhanced NO2 Gas-Sensing Properties of Au-Ag Bimetal Decorated MWCNTs/WO3 Composite Sensor under UV-LED Irradiation. *Sensors and Actuators A: Physical* **2020**, *303*, 111718.
(10) Hong, H. S.; Phuong, N. H.; Huong, N. T.; Nam, N. H.; Hue, N. T. Highly Sensitive and Low Detection Limit of Resistive NO2 Gas Sensor Based on a MoS2/Graphene Two-Dimensional Heterostructures. *Appl. Surf. Sci.* **2019**, *492*, 449−454.
(11) Ko, G.; Kim, H. Y.; Ahn, J.; Park, Y. M.; Lee, K. Y.; Kim, J. Graphene-Based Nitrogen Dioxide Gas Sensors. *Curr. Appl. Phys.* **2010**, *10* (4), 1002−1004.
(12) Nazemi, H.; Joseph, A.; Park, J.; Emadi, A. Advanced Micro- and Nano-Gas Sensor Technology: A Review. *Sensors 2019, Vol. 19, Page 1285* **2019**, *19* (6), 1285.
(13) Chua, X. J.; Luxa, J.; Eng, A. Y. S.; Tan, S. M.; Sofer, Z.; Pumera, M. Negative Electrocatalytic Effects of P-Doping Niobium and Tantalum on MoS_2 and WS_2 for the Hydrogen Evolution Reaction and Oxygen Reduction Reaction. *ACS Catal.* **2016**, *6* (9), 5724−5734.
(14) Zheng, W.; Xu, Y.; Zheng, L.; Yang, C.; Pinna, N.; Liu, X.; Zhang, J. MoS_2 Van Der Waals p−n Junctions Enabling Highly Selective Room-Temperature NO_2 Sensor. *Adv. Funct. Mater.* **2020**, *30* (19), 2000435.
(15) Pham, T.; Li, G.; Bekyarova, E.; Itkis, M. E.; Mulchandani, A. MoS2-Based Optoelectronic Gas Sensor with Sub-Parts-per-Billion Limit of NO_2 Gas Detection. *ACS Nano* **2019**, *13* (3), 3196−3205.
(16) Park, J.; Mun, J.; Shin, J.-S.; Kang, S.-W. Highly Sensitive Two-Dimensional MoS_2 Gas Sensor Decorated with Pt Nanoparticles. *R. Soc. Open Sci.* **2018**, *5* (12), 181462.
(17) Baek, D. H.; Kim, J. MoS_2 Gas Sensor Functionalized by Pd for the Detection of Hydrogen. *Sens. Actuators, B* **2017**, *250*, 686−691.
(18) Hung, C. M.; Vuong, V. A.; Duy, N. V.; An, D. V.; Hieu, N. V.; Kashif, M.; Hoa, N. D. Controlled Growth of Vertically Oriented Trilayer MoS_2 Nanoflakes for Room-Temperature NO_2 Gas Sensor Applications. *physica status solidi (a)* **2020**, *217* (12), 2000004.
(19) Singh, E.; Singh, P.; Kim, K. S.; Yeom, G. Y.; Nalwa, H. S. Flexible Molybdenum Disulfide (MoS_2) Atomic Layers for Wearable Electronics and Optoelectronics. *ACS Appl. Mater. Interfaces* **2019**, *11* (12), 11061−11105.
(20) Zhu, J.; Zhang, H.; Tong, Y.; Zhao, L.; Zhang, Y.; Qiu, Y.; Lin, X. First-Principles Investigations of Metal (V, Nb, Ta)-Doped Monolayer MoS_2: Structural Stability, Electronic Properties and Adsorption of Gas Molecules. *Appl. Surf. Sci.* **2017**, *419*, 522−530.
(21) Xiao, Z.; Wu, W.; Wu, X.; Zhang, Y. Adsorption of NO_2 on Monolayer MoS_2 Doped with Fe, Co, and Ni, Cu: A Computational Investigation. *Chem. Phys. Lett.* **2020**, *755*, 137768.
(22) Wang, T.; Gao, D.; Zhuo, J.; Zhu, Z.; Papakonstantinou, P.; Li, Y.; Li, M. Size-Dependent Enhancement of Electrocatalytic Oxygen-Reduction and Hydrogen-Evolution Performance of MoS_2 Particles. *Chem. Eur. J.* **2013**, *19* (36), 11939−11948.
(23) Suh, J.; Park, T.-E.; Lin, D.-Y.; Fu, D.; Park, J.; Jung, H. J.; Chen, Y.; Ko, C.; Jang, C.; Sun, Y.; Sinclair, R.; Chang, J.; Tongay, S.; Wu, J. Doping against the Native Propensity of MoS_2: Degenerate Hole Doping by Cation Substitution. *Nano Lett.* **2014**, *14* (12), 6976−6982.
(24) Robertson, A. W.; Lin, Y.-C.; Wang, S.; Sawada, H.; Allen, C. S.; Chen, Q.; Lee, S.; Lee, G.-D.; Lee, J.; Han, S.; Yoon, E.; Kirkland, A. I.; Kim, H.; Suenaga, K.; Warner, J. H. Atomic Structure and Spectroscopy of Single Metal (Cr, V) Substitutional Dopants in Monolayer MoS_2. *ACS Nano* **2016**, *10* (11), 10227−10236.
(25) Li, M.; Yao, J.; Wu, X.; Zhang, S.; Xing, B.; Niu, X.; Yan, X.; Yu, Y.; Liu, Y.; Wang, Y. P-Type Doping in Large-Area Monolayer MoS_2 by Chemical Vapor Deposition. *ACS Appl. Mater. Interfaces* **2020**, *12* (5), 6276−6282.
(26) Sohn, A.; Kim, C.; Jung, J.-H.; Kim, J. H.; Byun, K.-E.; Cho, Y.; Zhao, P.; Kim, S. W.; Seol, M.; Lee, Z.; Kim, S.-W.; Shin, H.-J. Precise Layer Control and Electronic State Modulation of a Transition Metal Dichalcogenide via Phase-Transition-Induced Growth. *Adv. Mater.* **2021**, 2103286.

(27) Jin, Y.; Zeng, Z.; Xu, Z.; Lin, Y.-C.; Bi, K.; Shao, G.; Hu, T. S.; Wang, S.; Li, S.; Suenaga, K.; Duan, H.; Feng, Y.; Liu, S. Synthesis and Transport Properties of Degenerate P-Type Nb-Doped WS_2 Monolayers. *Chem. Mater.* **2019**, *31* (9), 3534−3541.
(28) Qin, Z.; Loh, L.; Wang, J.; Xu, X.; Zhang, Q.; Haas, B.; Alvarez, C.; Okuno, H.; Yong, J. Z.; Schultz, T.; Koch, N.; Dan, J.; Pennycook, S. J.; Zeng, D.; Bosman, M.; Eda, G. Growth of Nb-Doped Monolayer WS_2 by Liquid-Phase Precursor Mixing. *ACS Nano* **2019**, *13* (9), 10768−10775.
(29) Ivanovskaya, V. v.; Zobelli, A.; Gloter, A.; Brun, N.; Serin, V.; Colliex, C. Ab Initio Study of Bilateral Doping within the the MoS_2-NbS_2. *Phys. Rev. B* **2008**, *78* (13), 134104.
(30) Zhang, D.; Wu, Y.-C.; Yang, M.; Liu, X.; Coileáin, C. Ó.; Abid, M.; Abid, M.; Wang, J.-J.; Shvets, I.; Xu, H.; Chun, B. S.; Liu, H.; Wu, H.-C. Surface Enhanced Raman Scattering of Monolayer MX_2 with Metallic Nano Particles. *Scientific Reports 2016 6:1* **2016**, *6* (1), 1−8.
(31) Ho, Y.-T.; Ma, C.-H.; Luong, T.-T.; Wei, L.-L.; Yen, T.-C.; Hsu, W.-T.; Chang, W.-H.; Chu, Y.-C.; Tu, Y.-Y.; Pande, K. P.; Chang, E. Y. Layered MoS_2 Grown on c -Sapphire by Pulsed Laser Deposition. *Phys. Status Solidi RRL* **2015**, *9* (3), 187−191.
(32) Joseph, D.; Navaneethan, M.; Abinaya, R.; Harish, S.; Archana, J.; Ponnusamy, S.; Hara, K.; Hayakawa, Y. Thermoelectric Performance of Cu-Doped MoS_2 Layered Nanosheets for Low Grade Waste Heat Recovery. *Appl. Surf. Sci.* **2020**, *505*, 144066.
(33) Silambarasan, K.; et al. One-Step Fabrication of Ultrathin Layered 1T@2H Phase MoS_2 with High Catalytic Activity Based Counter Electrode for Photovoltaic Devices. *Journal of Materials Science & Technology* **2020**, *51*, 94−101.
(34) Gao, D.; Si, M.; Li, J.; Zhang, J.; Zhang, Z.; Yang, Z.; Xue, D. Ferromagnetism in Freestanding MoS_2 Nanosheets. *Nanoscale Research Letters 2013 8:1* **2013**, *8* (1), 1−8.
(35) Zhao, L.; Jia, J.; Yang, Z.; Yu, J.; Wang, A.; Sang, Y.; Zhou, W.; Liu, H. One-Step Synthesis of CdS Nanoparticles/MoS_2 Nanosheets Heterostructure on Porous Molybdenum Sheet for Enhanced Photocatalytic H_2 Evolution. *Applied Catalysis B: Environmental* **2017**, *210*, 290−296.
(36) Ji, H.; Hu, S.; Shi, S.; Guo, B.; Hou, W.; Yang, G. Rapid Microwave-Hydrothermal Preparation of Few-Layer MoS_2/C Nanocomposite as Anode for Highly Reversible Lithium Storage Properties. *Journal of Materials Science 2018 53:20* **2018**, *53* (20), 14548−14558.
(37) McDonnell, S.; Addou, R.; Buie, C.; Wallace, R. M.; Hinkle, C. L. Defect-Dominated Doping and Contact Resistance in MoS_2. *ACS Nano* **2014**, *8* (3), 2880−2888.
(38) Deepak, F. L.; Cohen, H.; Cohen, S.; Feldman, Y.; Popovitz-Biro, R.; Azulay, D.; Millo, O.; Tenne, R. Fullerene-Like (IF) $NbxMo_1$-XS_2 Nanoparticles. *J. Am. Chem. Soc.* **2007**, *129* (41), 12549−12562.
(39) Kumar, R. R.; Habib, M. R.; Khan, A.; Chen, P.-C.; Murugesan, T.; Gupta, S.; Anbalagan, A. k.; Tai, N.-H.; Lee, C.-H.; Lin, H.-N. Sulfur Monovacancies in Liquid-Exfoliated MoS_2 Nanosheets for NO_2 Gas Sensing. *ACS Applied Nano Materials* **2021**, *4* (9), 9459−9470.
(40) Cho, B.; Hahm, M. G.; Choi, M.; Yoon, J.; Kim, A. R.; Lee, Y.-J.; Park, S.-G.; Kwon, J.-D.; Kim, C. S.; Song, M.; Jeong, Y.; Nam, K.-S.; Lee, S.; Yoo, T. J.; Kang, C. G.; Lee, B. H.; Ko, H. C.; Ajayan, P. M.; Kim, D.-H. Charge-Transfer-Based Gas Sensing Using Atomic-Layer MoS_2. *Scientific Reports 2015 5:1* **2015**, *5* (1), 1−6.
(41) Long, H.; Chan, L.; Harley-Trochimczyk, A.; Luna, L. E.; Tang, Z.; Shi, T.; Zettl, A.; Carraro, C.; Worsley, M. A.; Maboudian, R. 3D MoS_2 Aerogel for Ultrasensitive NO_2 Detection and Its Tunable Sensing Behavior. *Advanced Materials Interfaces* **2017**, *4* (16), 1700217.
(42) He, Q.; Zeng, Z.; Yin, Z.; Li, H.; Wu, S.; Huang, X.; Zhang, H. Fabrication of Flexible MoS2 Thin-Film Transistor Arrays for Practical Gas-Sensing Applications. *Small* **2012**, *8* (19), 2994−2999.
(43) Niu, Y.; Wang, R.; Jiao, W.; Ding, G.; Hao, L.; Yang, F.; He, X. MoS_2 Graphene Fiber Based Gas Sensing Devices. *Carbon* **2015**, *95*, 34−41.
(44) Yu, L.; Guo, F.; Liu, S.; Qi, J.; Yin, M.; Yang, B.; Liu, Z.; Fan, X. H. Hierarchical 3D Flower-like MoS_2 Spheres: Post-Thermal Treatment in Vacuum and Their NO_2 Sensing Properties. *Mater. Lett.* **2016**, *183*, 122−126.
(45) Cho, B.; Yoon, J.; Lim, S. K.; Kim, A. R.; Kim, D.-H.; Park, S.-G.; Kwon, J.-D.; Lee, Y.-J.; Lee, K.-H.; Lee, B. H.; Ko, H. C.; Hahm, M. G. Chemical Sensing of 2D Graphene/MoS_2 Heterostructure Device. *ACS Appl. Mater. Interfaces* **2015**, *7* (30), 16775−16780.
(46) Neetika; Kumar, A.; Chandra, R.; Malik, V. K. MoS_2 Nanoworm Thin Films for NO_2 Gas Sensing Application. *Thin Solid Films* **2021**, *725*, 138625.
(47) Kumar, R.; Goel, N.; Kumar, M. High Performance NO_2 Sensor Using MoS_2 Nanowires Network. *Appl. Phys. Lett.* **2018**, *112* (5), 053502.
(48) Sun, J.; Muruganathan, M.; Mizuta, H. Room Temperature Detection of Individual Molecular Physisorption Using Suspended Bilayer Graphene. *Sci. Adv.* **2016**, *2* (4), 1501518 DOI: 10.1126/sciadv.1501518.
(49) Muruganathan, M.; Sun, J.; Imamura, T.; Mizuta, H. Electrically Tunable van Der Waals Interaction in Graphene−Molecule Complex. *Nano Lett.* **2015**, *15* (12), 8176−8180.
(50) Agbonlahor, O. G.; Muruganathan, M.; Imamura, T.; Mizuta, H. Adsorbed Molecules as Interchangeable Dopants and Scatterers with a Van Der Waals Bonding Memory in Graphene Sensors. *ACS Sensors* **2020**, *5* (7), 2003−2009.
(51) Smidstrup, S.; Stradi, D.; Wellendorff, J.; Khomyakov, P. A.; Vej-Hansen, U. G.; Lee, M.-E.; Ghosh, T.; Jónsson, E.; Jónsson, H.; Stokbro, K. First-Principles Green's-Function Method for Surface Calculations: A Pseudopotential Localized Basis Set Approach. *Phys. Rev. B* **2017**, *96* (19), 195309.
(52) Smidstrup, S.; Markussen, T.; Vancraeyveld, P.; Wellendorff, J.; Schneider, J.; Gunst, T.; Verstichel, B.; Stradi, D.; Khomyakov, P. A.; Vej-Hansen, U. G.; Lee, M.-E.; Chill, S. T.; Rasmussen, F.; Penazzi, G.; Corsetti, F.; Ojanperä, A.; Jensen, K.; Palsgaard, M. L. N.; Martinez, U.; Blom, A.; Brandbyge, M.; Stokbro, K. QuantumATK: An Integrated Platform of Electronic and Atomic-Scale Modelling Tools. *J. Phys.: Condens. Matter* **2020**, *32* (1), 015901.
(53) Grimme, S.; Antony, J.; Ehrlich, S.; Krieg, H. A Consistent and Accurate Ab Initio Parametrization of Density Functional Dispersion Correction (DFT-D) for the 94 Elements H-Pu. *J. Chem. Phys.* **2010**, *132* (15), 154104.
(54) *Atomistic Simulation Software QuantumATK - Synopsys*. https://www.synopsys.com/silicon/quantumatk.html (accessed 2021-10-22).
(55) Nundy, S.; Eom, T.-y.; Kang, J.-g.; Suh, J.; Cho, M.; Park, J.-S.; Lee, H.-J. Flower-Shaped ZnO Nanomaterials for Low-Temperature Operations in NOX Gas Sensors. *Ceram. Int.* **2020**, *46* (5), 5706−5714.
(56) Sankar ganesh, R.; Navaneethan, M.; Mani, G. K.; Ponnusamy, S.; Tsuchiya, K.; Muthamizhchelvan, C.; Kawasaki, S.; Hayakawa, Y. Influence of Al Doping on the Structural, Morphological, Optical, and Gas Sensing Properties of ZnO Nanorods. *J. Alloys Compd.* **2017**, *698*, 555−564.

https://doi.org/10.1021/acsomega.1c07274
ACS Omega 2022, 7, 10492−10501